NUKLEONIKA 2006;51(2):131–135

TECHNICAL NOTE

A radiographic facility at the Soltan Institute for Nuclear Studies (SINS) at Świerk, Poland

**Jerzy Bigolas,
Wojciech Drabik,
Eugeniusz Pławski,
Anna Wysocka-Rabin**

Abstract This paper describes the 6 MeV linac electron accelerator facility now operating at SINS, Świerk, Poland. The accelerator can work in both the electron or X-ray photon mode. The photon beam may be used for non-destructive radiographic investigations on a laboratory scale and, with some modifications, for industrial purposes, as well. As the accelerator's removable tungsten e/X converter is placed outside, the beam vacuum window, an external electron beam is also accessible. The design stages of the accelerator's construction are described, and examples of measurements and radiographic pictures are also presented.

Key words linear accelerator • electron RF accelerator • photon beam • radiography

Introduction

At present, the IAEA estimates that worldwide there are more than 15,000 small energy (up to 20 MeV) accelerators, most of which are electron linacs. They are used extensively for beneficial purposes, in medical, industrial, agricultural, research and educational applications.

In Poland, the number of electron accelerator units is far below that of most industrial nations, and almost all of them are radio-therapeutic units. However, SINS has the comprehensive knowledge and technical capacity to build accelerators for industrial applications.

The radiographic facility built and tested over the last two years in the Accelerator Physics and Technology Department at SINS consists of electron accelerator and e/X conversion units placed in a radiation shielded concrete room. The e/X conversion area is equipped additionally with 10 cm lead shields surrounding the conversion head and exposure compartment. The SINS electron accelerator is based on a linear RF accelerating structure composed of 11 on-axis coupled cells working in the *S* band at a frequency of 3 GHz.

The accelerator is excited in the so-called $\pi/2$ mode, where dimensional tolerances are strongly relaxed compared to the standard π mode. Electrons are injected from the thermionic diode gun pulsed together with an RF power source exciting the accelerating structure.

The accelerated electron beam passes into the air through a thin (40 μm stainless steel) vacuum window. The water-cooled, removable e/X conversion head holding the tungsten target can be placed few

J. Bigolas, W. Drabik, E. Pławski✉, A. Wysocka-Rabin
Accelerator Physics and Technology Department,
The Andrzej Soltan Institute for Nuclear Studies,
05-400 Otwock-Świerk, Poland,
Tel.: +48 22 718 05 40, Fax: +48 22 779 34 81,
E-mail: plawski@ipj.gov.pl

Received: 25 July 2005
Accepted: 24 January 2006

Table 1. Accelerator components and parameters

Electron gun	Diode, cylindrical Pierce geometry type, thermionic tungsten cathode Energy/intensity: 30 keV/200 mA in pulse 4 μs Variable repetition: 50–300 Hz
RF accelerating structure	11 cells, on axis coupled π/2 mode Resonant frequency: 2997.85 MHz Quality factor: 12,500 Average accelerating field: 15 MV/m (peak 23 MV/m) RF power lost to walls: 1.2 MW in 4 μs pulse Nominal energy: 6 MeV Electron current: 100 mA in pulse, 0.1 mA average Structure length (total): 50 cm Working temperature: 40 ± 1°C
Beam focusing and steering	Solenoid surrounding the accelerating structure: iron screened 10 cm inner diam coil of 45 cm length; maximum attainable axial magnetic field 700 Gs Magnetic quadrupole doublet on structure output Beam position correctors: two pairs of small coils underneath the solenoid coil
e/X conversion unit (tungsten target) – radiographic parameters	Electron beam energy: 6 MeV Focal spot: 2 mm maximum X-ray dose rate: 500 R/min/m Flaw detectability: 0.4%

millimetres downstream from this window. Thus, the facility can be operated in either the electron beam mode or X-ray beam mode depending on demand.

Accelerator design

The basic components and parameters of the accelerator are listed in Table 1. The flaw detectability given in Table 1 was determined aproximately according to the definition of flaw detectability. We have prepared steel cylinder, 100 mm in height and 150 mm in diameter. On the one base of the cylinder we made thin rows with different depths: 0.2, 0.4, 0.6, 0.8, 1, 2, 3, 4 mm. The width of each row was fixed at 1.5 mm. This pattern was exposed to the X-ray beam along the axis of the cylinder and the radiographs of these rows were detected on a Kodak Industrex A-400 film. The flaw detectability was calculated as ratio of the minimum depth of the visible row to the thickness of cylinder. During the future examination of industrial samples the image quality verification using IQI according to EN462-2 is predicted.

Design calculations and optimisation

A thorough computational optimisation of the electron gun and successive RF accelerating structure preceded the construction of the accelerator. In order to obtain the optimum shapes of structures, computational DC [4] and RF [2] codes were checked with beam dynamics codes developed in our Institute. Samples of final computational results are presented in Figs. 1, 2 and 3.

RF accelerating structure and auxiliaries

Components of the RF accelerating structures are fabricated from a certified OFHC copper. The guaranteed Cu content of this material exceeds 99.995%, while its oxygen content is below 1.0 ppm.

Two fabricating options were available: brazing in a vacuum or brazing in a hydrogen atmosphere. In the

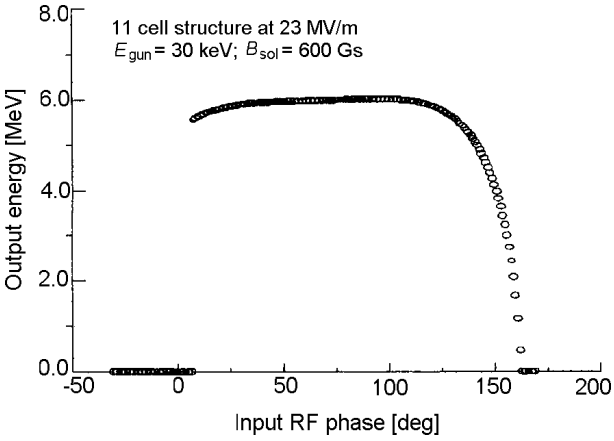

Fig. 1. Computed phase acceptance of the accelerating structure: 23 MV/m amplitude corresponds to 15 MV/m mean field.

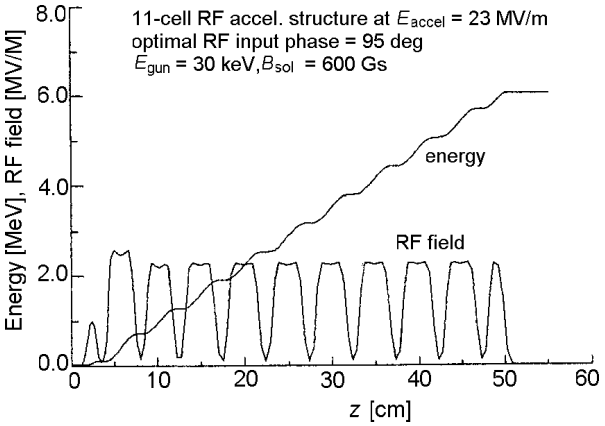

Fig. 2. Electron beam transmission through RF accelerating structure at optimal input phase 95°RF.

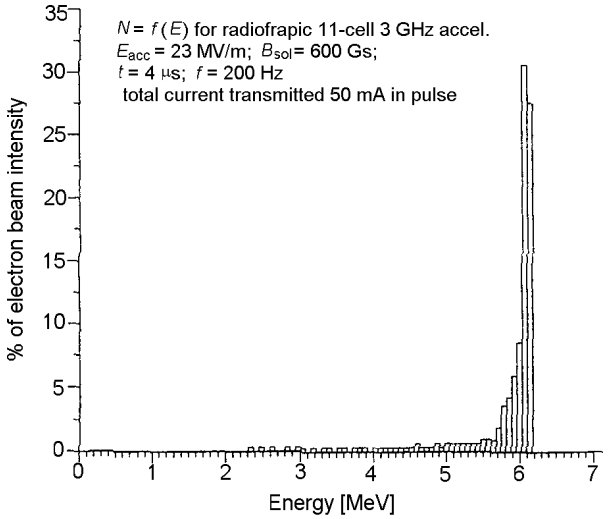

Fig. 3. Calculated electron energy spectrum on *W* target of radiographic 6 MeV accelerator. Beam diameter on target: 2 mm. Target thickness/diameter: 1 mm/10 mm.

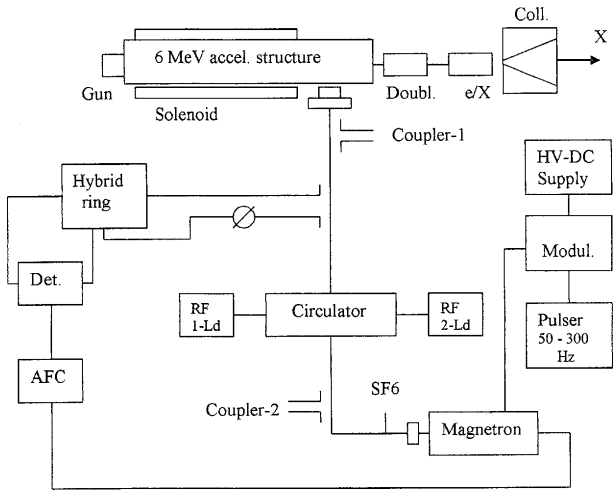

Fig. 4. Schematic lay-out of a radiographic facility.

first case, the grain size of copper is more critical, while in the second the content of oxygen is very important. The structure actually mounted in a radiographic facility was brazed in a vacuum oven.

After the last brazing operation, the whole structure was tuned to the working π/2 mode. The Slater perturbation method was applied with a metal perturbing bead moved on the axis. A block diagram of the structure is shown in Fig. 4.

The RF power-exciting electromagnetic field in the accelerating structure is generated by a 2999 MHz, 2 MW in-pulse magnetron, and is delivered to the coupling window of the accelerating structure via the pressurised WR284 waveguide system. This system consists of a 4-way circulator, RF power loads and various RF sensing and regulation devices, as also shown in Fig. 4. An automatic frequency tuning (AFC) system tunes the magnetron to the structure frequency.

A photograph of the accelerator with its RF, vacuum and cooling systems is shown in Fig. 5.

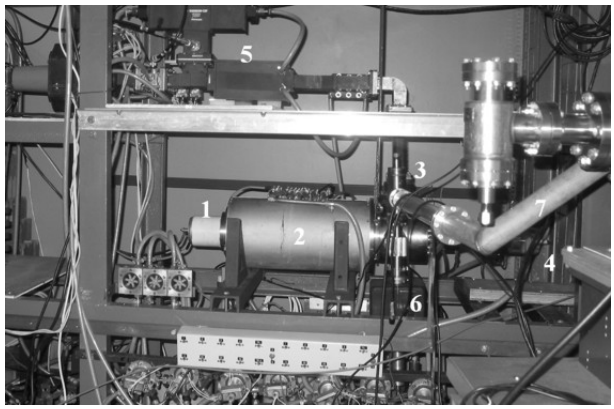

Fig. 5. 6 MeV electron linac mounted in shielded bunker. 1 – diode electron gun; 2 – RF accelerating structure placed in focusing solenoid; 3 – RF power input to accelerating structure; 4 – electron beam output vacuum window; 5 – RF power supply system (magnetron + RF circulator + RF directional couplers); 6 – vacuum ion pump; 7 – auxiliary vacuum pumping system.

Electron beam spectra measurements

In the electron mode, measurements of the electron beam spectra are made using a simple magnetic analyser. First, the electron beam emerging from the accelerating structure is deflected by 60 degrees in the magnetic field of the analyser. Then, after passing through the energy defining slit, it is collected in the Faraday cup. The current of the Faraday cup is converted to a voltage signal and measured with an oscilloscope.

Electron beam energy is determined by the relationship between magnetic field intensity and energy. The result is verified by calculations of electron beam trajectories in the magnetic gap, taking into account fringe effects.

In Figure 6, the shape of the spectrum is drawn for a magnetron parameter of $U_m = 4$ VA, with an electron beam of $I_e = 6$ mA in 4 μs pulse.

The main difference between the theoretical and measured spectrum is broadening of the measured spectrum compare to the theoretical one. The broadening of the experimental spectrum is caused by several reasons:

– finite size of the electron beam,
– finite size of input slit of the magnetic analyzer (limiting aperture),

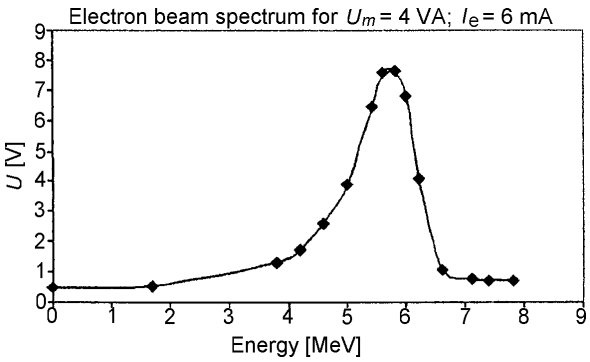

Fig. 6. Measured electron energy spectrum of the radiographic accelerator.

- finite size of output slit of magnetic analyzer (energy definition slit),
- pulsations of the current in magnetic coils,
- magnetic field measurements errors (magnetization curve),
- electronic noise due to RF magnetron generator.

Monte Carlo calculations of the photon beam

The Monte Carlo code BEAMnrc/EGSnrc [5], was used to calculate spectral distribution, mean energy distribution and fluence vs. position for a photon beam in the radiographic accelerator.

Calculations were done for 7×10^7 particles, using an electron transport cutoff of ECUT = 0.7 MeV, and a photon transport cutoff of PCUT = 0.01 MeV. A value of 0.25 was used to obtain the lowest possible fractional electron energy loss per step (ESTEPE). Relativistic spin effects were included in nuclear elastic scattering to obtain accurate calculations near high-Z interfaces. The electron step algorithm PRESTA-II (an essential requirement for accurate high-Z interface simulations) and the exact boundary crossing algorithm, BCA PRESTA-I, were also implemented.

The source type of incident electron beam in the BEAMnrc code was a Parallel Circular Beam with 2-D Gaussian X-Y distribution. The value of FWHM in the Gaussian distribution was set at 2 mm. The energy spectrum of the electron beam was set from 2.3 to 6.25 MeV (see Fig. 3). A tungsten target of 6 mm diameter and 1 mm thickness was used as the e^-/X conversion unit. The influence of different energy spectra of electrons was then investigated.

Phase space files (PHSP) were generated for scoring planes at different distances from the tungsten target. The PHSP contain data relating to particle position, direction, charge, and other key parameters for every particle crossing the scoring plane. The BEAMDP program was used for processing phase space files and to derive spectral distribution, mean energy distribution and fluence vs. position of a photon beam in air.

Figures 7 and 8 show the energy spectrum and fluence vs. position of a photon beam for a field area with a radius of 10 cm, at a distance of 100 cm from the tungsten target. Photon fluence is normalised by the energy bin width,

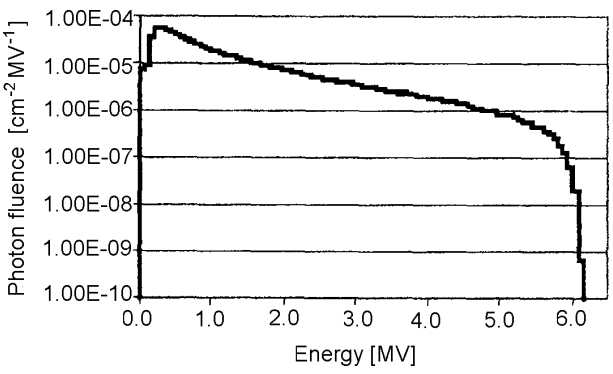

Fig. 7. The energy spectrum of a photon beam in air for a field area with a radius of 10 cm at a distance of 100 cm from the tungsten target.

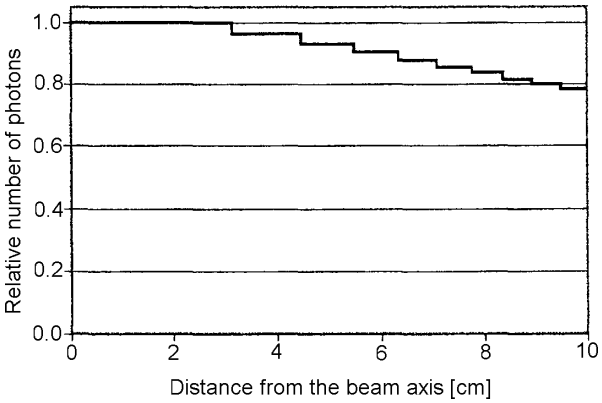

Fig. 8. Fluence vs. position of a photon beam in air for a field area with a radius of 10 cm at a distance of 100 cm from the tungsten target.

number of incident particles, and the area of the field being considered. The mean energy of photon beam changes was from 1.18 MV to 1.14 MV, at a distance of 10 cm from the beam axis.

Radiographic pictures

A Kodak Industrex AA 400 film was chosen for radiographic images. Experiments were performed with different exposures and filters to obtain good radiographic contrast.

The radiographic images of two different specimens are presented in Figs. 9 and 10. Flaw detectability was 0.4%. In radiographic practice, this term denotes the ratio of the thickness of the smallest detectable flaw to the thickness of the object under inspection, expressed as a percentage.

Fig. 9. Radiographic image of the diode electron gun.

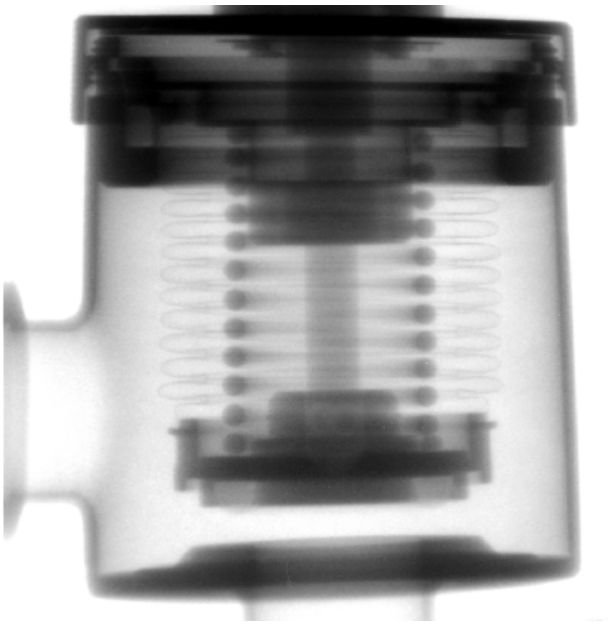

Fig. 10. Radiographic image of the vacuum valve.

Conclusions

The SINS 6 MeV electron accelerator unit, based on a standing wave *S*-band resonant structure, was built successfully and has passed preliminary tests. Since it is foreseen primarily as a radiographic device, a number of steps have been taken to optimise its advantages in these applications. After optimisation of accelerator parameters, the radiographic images of different objects on Kodak films are of excellent quality.

The electron beam has been used, as well. The Research Team S1 (Dosimetry of Mixed Radiation) has used our 6 MeV electron beam to study the behaviour and ion collection efficiency of gaseous ionisation chambers used in dosimetry [3]. Apart from radiography [1], the 6 MeV accelerator may also prove to be a very useful research device for detector calibration, drug and explosive detection.

References

1. Bigolas J, Kuliński S, Pachan M *et al*. (1994) The Lillyput – mobile electron linear accelerator for radiography and its use in testing of civil engineering objects. In: Proc of the 4th European Particle Accelerator Conf EPAC'94, 27 June – 1 July 1994. World Scientific, Singapore, pp 2658–2660
2. Billen JH, Young LM (1996) Poisson-superfish. Los Alamos Report LA-UR-96-1834
3. Golnik N, Kamiński P, Zielczyński M (2004) A measuring system with a recombination chamber for neutron dosimetry around medical accelerators. Radiat Prot Dosim 110:273–276
4. Herrmansfeld WB (1988) E-Gun Code. SLAC-331/1988 Report. Stanford University, Stanford, California
5. Kawrakow I, Rogers DWO (2001) The EGSnrc Code System: Monte Carlo simulation of electron and photon transport. National Research Council of Canada Report no. PIRS-701